JOURNAL OF GEOPHYSICAL RESEARCH: ATMOSPHERES, VOL. 118, 329–339, doi:10.1029/2012JD018053, 2013

Evaluation of the atmospheric water vapor content in a regional climate model using ground-based GPS measurements

T. Ning,[1] G. Elgered,[1] U. Willén,[2] and J. M. Johansson[1]

Received 6 May 2012; revised 18 October 2012; accepted 7 December 2012; published 17 January 2013.

[1] Ground-based GPS measurements can provide independent data for the assessment of climate models. We use the atmospheric integrated water vapor (IWV) obtained from GPS measurements at 99 European sites to evaluate the regional Rossby Centre Atmospheric climate model (RCA) driven at the boundaries by the European Centre for Medium-Range Weather Forecasts (ECMWF) reanalysis data (ERA Interim). The GPS data were compared to the RCA simulation and the ERA Interim data. The comparison was first made using the monthly mean values. Averaged over the domain and the 14 years covered by the GPS data, IWV differences of about 0.47 kg/m^2 and 0.39 kg/m^2 are obtained for RCA-GPS and ECMWF-GPS, respectively. The RCA-GPS standard deviation is 0.98 kg/m^2 whereas it is 0.35 kg/m^2 for the ECMWF-GPS comparison. The IWV differences for RCA are positively correlated to the differences for ECMWF. However, this is not the case for two sites in Italy where a wet bias is seen for ECMWF, while a dry bias is seen for RCA, the latter being consistent with a cold temperature bias found for RCA in that region by other authors. Comparisons of the estimated diurnal cycle and the spatial structure function of the IWV were made between the GPS data and the RCA simulation. The RCA captures the geographical variation of the diurnal peak in the summer. Averaged over all sites, a peak at 17 local solar time is obtained from the GPS data while it appears later, at 18, in the RCA simulation. The spatial variation of the IWV obtained for an RCA run with a resolution of 11 km gives a better agreement with the GPS results than does the spatial variation from a 50 km resolution run.

Citation: Ning, T., G. Elgered, U. Willén, and J. M. Johansson (2013), Evaluation of the atmospheric water vapor content in a regional climate model using ground-based GPS measurements, *J. Geophys. Res. Atmos.*, *118*, 329–339, doi:10.1029/2012JD018053.

1. Introduction

[2] Water is found on the Earth in three states: vapor, liquid, and solid. It is constantly changing between these states due to evaporation and condensation, which in turn significantly affects the Earth's climate system. In addition to its role in the hydrological cycle, the atmospheric water vapor is also an efficient greenhouse gas and is one of the most important constituents in climate feedback processes [*Cess et al*., 1990; *Held and Soden*, 2000; *Semenov and Bengtsson*, 2002]. A warmer climate increases the amount of water vapor in the atmosphere causing a positive feedback meaning that more outgoing long-wave radiation is absorbed and reemitted back to the ground. Therefore, a good knowledge about the water vapor content of the atmosphere—in the following referred to as integrated water vapor (IWV)—is crucial in climate research. The IWV in the past and the present climate, and its future changes are simulated by climate models. Based on an investigation of eight regional climate models, using reanalysis boundary conditions, *Wyser et al*. [2008] found that the IWV can be reasonably well simulated at monthly and daily time scales, but with considerable differences between individual models. The IWV simulation from regional climate models run with reanalysis boundary fields will differ from the IWV given by reanalysis data due to the data assimilation, which keeps the reanalysis data closer to the observations. The reanalysis data may be used to evaluate simulations of the IWV values. However, it is not always suitable for climate applications over long time periods due to changes in the observing systems [*Bengtsson et al*., 2004]. Therefore, it is also important to evaluate climate model simulations using accurate and independent IWV observations.

[3] Traditionally, the long-term variation of the atmospheric IWV is monitored using radiosonde measurements [*Ross and Elliott*, 1996, 2001], which are also assimilated in the weather forecasting model to provide reanalysis products [*Uppala et al*., 2005]. However, the accuracy of the radiosonde-derived IWV is limited by the sensor characteristics that vary in space

[1]Department of Earth and Space Sciences, Chalmers University of Technology, Onsala Space Observatory, SE-43992, Onsala, Sweden.
[2]Swedish Meteorological and Hydrological Institute, SE-60176, Norrköping, Sweden.

Corresponding author: T. Ning, Department of Earth and Space Sciences, Chalmers University of Technology, Onsala Space Observatory, SE-43992 Onsala, Sweden. (tongn@chalmers.se)

2169-897X/13/2012JD018053

and time [*Wang and Zhang*, 2008]. Meanwhile, the instrumental stability also varies (e.g., due to sensor changes), which may introduce offsets in the measured IWV. This limits the role of the radiosonde data for climate research [*Titchner et al.*, 2009]. Satellite-based measurements are able to provide IWV globally using remote sensing methods observing in the infrared and the optical frequency bands [*Chaboureau et al.*, 1998] or using microwave remote sensing techniques [*Jury and Waliser*, 1990]. Satellite observations are also based on different instruments over long time periods and they may not provide data under all weather conditions.

[4] More recently, the IWV has been inferred from the ground-based measurements of the GPS based on the path delay of radio signals that propagate through the neutral atmosphere. Given the ability of operating under almost all weather conditions and the long-term stability, the GPS technique has a superiority to measure long time series of the IWV with a temporal resolution as high as a few minutes [*Wang and Zhang*, 2009]. GPS receivers are increasing in numbers globally and locally, providing an improved spatial resolution of the GPS-derived IWV. In addition, in difference to the radiosonde data, the ground-based GPS data have not yet been assimilated in the climate reanalysis products (European Centre for Medium-Range Weather Forecasts (ECMWF) ERA Interim used in this work), meaning that they offer an independent data set suitable for the evaluation of climate models. Furthermore, by applying a reprocessing strategy, it is possible to obtain homogenous GPS-derived IWV time series; see, e.g., *Gradinarsky et al.* [2002] and *Vey et al.* [2009, 2010], for the evaluation of climate models over long time periods.

[5] This work addresses the use of the IWV from ground-based GPS data for an assessment of the quality of a regional climate model used for simulations of present and future climate conditions in Europe. Section 2 describes the data analysis to infer the IWV and how the gridded model values are compared to the GPS-derived IWV. To investigate the quality of the IWV estimates from GPS, an analysis to estimate the total uncertainty of the GPS-derived IWV is discussed in section 3. The results are presented in section 4, followed by the conclusions in section 5.

2. Data Sets and Analysis Procedures

2.1. GPS Data

[6] We used GPS measurements with a maximum length of 14 years (1 January 1997 to 31 December 2010) and a minimum length of 6 years (see Figure 1) acquired at 99 sites in Europe between latitudes 39°N and 71°N, and between longitudes –22°E and +31°E. The ionospheric free linear combinations were processed by GIPSY/OASIS II v.5.0 [*Webb and Zumberge*, 1993] using the precise point positioning strategy [*Zumberge et al.*, 1997]. The reprocessed satellite orbit and clock products were used (http://gipsyoasis.jpl.nasa.gov/gipsy/docs/GipsyUsersAGU2007.pdf). An a priori zenith total delay (ZTD) was first formed by the sum of an a priori zenith hydrostatic delay (ZHD) and an a priori zenith wet delay (ZWD). The a priori of ZHD was obtained using the model presented by *Saastamoinen* [1973] (a typical value for a site at the sea level is around 2.3 m), and a value of 0.1 m for the a priori ZWD was used for all

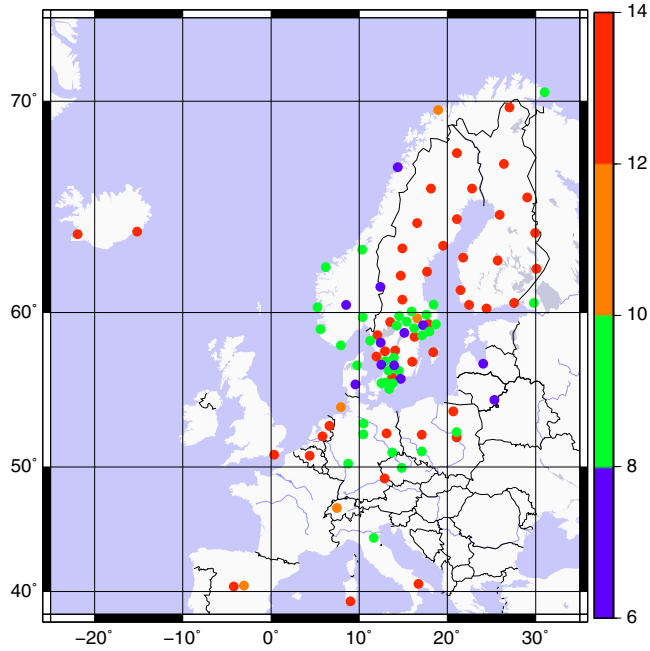

Figure 1. Length of the time series (in years) available for each GPS site. The circle denoting the site is color coded.

GPS sites. These empirical a priori values are often used in the GIPSY processing and are not critical for our application [*Thomas et al.*, 2011]. Corrections for the a priori ZTD together with the horizontal delay gradients were estimated using an elevation cutoff angle of 10° and updated every 5 min. The estimated ZTD was obtained by the sum of the a priori ZHD, the a priori ZWD, and the estimated correction.

[7] The Niell Mapping Functions were used to convert the zenith delay to the delay in the direction of the observation [*Niell*, 1996]. We also implemented the absolute calibration of the phase center variations for all antennas [*Schmid et al.*, 2007] and an ocean tide loading correction using the FES2004 model [*Lyard et al.*, 2006] in the data processing.

[8] To obtain the ZWD, Z_w, we subtracted the ZHD, Z_h, from the estimated ZTD, Z_t [*Elgered*, 1993]

$$Z_w = Z_t - Z_h \tag{1}$$

where the ZHD can be calculated by

$$Z_h = (2.2767 \pm 0.0015)\frac{P_0}{f(\lambda, H)} \tag{2}$$

and

$$f(\lambda, H) = \left(1 - 2.66{\cdot}10^{-3}\cos(2\lambda) - 2.8{\cdot}10^{-7}H\right) \tag{3}$$

where ZHD is in units of mm; P_0 is the ground pressure in hPa; λ and H are the site latitude in degrees and the height above the geoid in m, respectively. A derivation of equation (2) can be found in *Davis et al.* [1985]. The uncertainty $\pm$ 0.0015 mm/hPa was calculated assuming that all uncertainties of the input parameters are uncorrelated. We used the ground pressure obtained from the reanalysis product of

the ECMWF after the vertical interpolation of the model's pressure profile to the height of the GPS site. The uncertainty of the ECMWF-derived ground pressure was evaluated by *Heise et al*. [2009] where they compared the interpolated ground pressure from the ECMWF analysis to the local ground measurements at more than 60 globally distributed GPS sites using 1 year of data. The results revealed an agreement with an overall mean bias and a standard deviation of 0.0 and 0.9 hPa, respectively. We did a similar test, but only for the GPS site at the Onsala Space Observatory, using more than 10 years of data. The result shows a mean bias and a standard deviation of 0.1 and 0.6 hPa, respectively.

[9] We can describe the ratio between the ZWD and the IWV, V, by the parameter Q

$$V = \frac{Z_w}{Q} = \frac{Z_t - Z_h}{Q} \tag{4}$$

where Q is related to the atmospheric temperature and humidity profiles. It was given by *Askne and Nordius* [1987]

$$Q = 10^{-6}\rho_w R_w \left[\frac{k_3}{T_m} + k'_2\right] \tag{5}$$

where ρ_w is the density of liquid water; R_w is the specific gas constant of water vapor; and k_3 and k'_2 are constants determined from laboratory experiments of the refractivity. The values we used were given by *Bevis et al*. [1994]. The mean atmospheric temperature T_m can be estimated from the vertical profiles of the atmospheric temperature, T, and the partial pressure of water vapor, e, [e.g., *Bevis et al*., 1994; *Hagemann et al*., 2003; *Wang et al*., 2005]:

$$T_m = \frac{\int_0^\infty \frac{e(h)}{T(h)} dh}{\int_0^\infty \frac{e(h)}{T(h)^2} dh}. \tag{6}$$

[10] To obtain T_m for each GPS site, we used the vertical profiles of atmospheric temperature and humidity given by the reanalysis product of ECMWF. A root-mean-square difference of 1.1 K in T_m was found by *Wang et al*. [2005] based on global comparisons between the ECMWF reanalysis and radiosonde measurements using 6 years of data.

2.2. Rossby Centre Atmospheric Climate Model (RCA) and ECMWF Data

[11] The regional Rossby Centre Atmospheric climate model (RCA), developed at the Swedish Meteorological and Hydrological Institute, is a hydrostatic gridpoint model with semi-Lagrangian dynamics based on the numerical weather prediction model HIRLAM [*Undén et al*., 2002]. The RCA solution is relaxed toward the forcing boundary data across an eight point wide relaxation zone following the boundary formulation presented by *Davies* [1976], with a tanh-based relaxation function. Most physical parameterizations in RCA have been replaced or further developed for the model to operate in the climate mode in the 10–50 km resolution range [*Jones et al*., 2004]. The version of the model used in this work is RCA3, which includes a new land surface scheme where each model gridpoint is divided into subtiles depending on surface type, i.e., water, open land, forest, and snow [*Samuelsson et al*., 2006, 2011]. The evaporation fluxes for each tile are combined into a mean value, which affects the humidity above the gridpoint. Therefore, the dominating tile type will dominate the IWV value.

[12] For climate scenarios the RCA is run with global climate model fields at the boundaries to produce high resolution climate scenario data for impact studies. For model development the model is run for present-day climate using reanalysis data at the boundaries. For this work, RCA was run over Europe with a horizontal resolution of 50 km and 24 vertical levels with boundary data from the ECMWF reanalysis data (ERA Interim) with a horizontal resolution of 2.0° and with a temporal resolution of 6 h. The ECMWF temperature and humidity fields were interpolated in space (vertically and horizontally) and in time to the RCA grid at each time step (30 min). The RCA and ECMWF IWV were calculated at the gridpoint closest to the GPS site using the height of the GPS site.

[13] The uncertainty of the model simulated IWV has been assessed for the ECMWF reanalysis products. For older versions of reanalysis (e.g., ERA40), *Trenberth et al*. [2005] found that the values are reasonable over land and where there are data from radiosondes but with relatively large errors over oceans. For the more recent ERA-Interim that is used in this work, the agreement to observations is significantly improved [*Dee et al*., 2011]. The uncertainty of the model IWV, however, has so far not been assessed for RCA3. This work is one way to evaluate the quality of the model.

3. Uncertainty of the GPS IWV

[14] Before carrying out the evaluation, the uncertainty of the GPS-derived IWV is addressed. As discussed in section 2.1, the IWV is calculated from the ZTD, the ZHD, and the conversion factor Q. Therefore, we can determine the total uncertainty of the IWV using uncertainties associated with each input variable (assumed uncorrelated)

$$\sigma_V = \sqrt{\left(\frac{\sigma_{Z_t}}{Q}\right)^2 + \left(\frac{\sigma_{Z_h}}{Q}\right)^2 + \left(V\frac{\sigma_Q}{Q}\right)^2}. \tag{7}$$

[15] The uncertainty of the GPS-derived ZTD depends on many parameters, i.e., satellite orbit errors, unmodeled ionospheric delay, signal multipath, antenna related errors (e.g., phase center variations), and mapping functions. However, it is difficult to evaluate those factors separately and to find a unique method to combine all error sources together. For simplification, we adopt the claimed ZTD uncertainty (SD = 4 mm) from the International GNSS Service [*Byun and Bar-Sever*, 2009]. The value is a lower threshold of the ZTD uncertainty and is supported by the results presented by *Ning et al*. [2012] where the comparisons of a 10 year long time series of ZWD, estimated from GPS, geodetic very long baseline interferometry, and a water vapor radiometer data were carried out.

[16] Because the impact of the uncertainty of the latitude and the height is negligible (see equation (3)), the uncertainty of the ZHD is determined by the uncertainties of the ground pressure and the constant (2.2767 mm/hPa) in equation (2)

$$\sigma_{Z_h} = \sqrt{\left(\frac{P_0\sigma_c}{f(\lambda,H)}\right)^2 + \left(\frac{2.2767\sigma_{P_0}}{f(\lambda,H)}\right)^2}. \quad (8)$$

[17] The uncertainty of Q is mainly determined by the uncertainties of T_m, k_3, and k'_2. There are insignificant contributions of the uncertainties of ρ_w and R_w (< 0.1% of the total uncertainty)

$$\sigma_Q = 10^{-6}\rho_w R_w \sqrt{\left(\frac{\sigma_{k_3}}{T_m}\right)^2 + \sigma^2_{k'_2} + \left(k_3\frac{\sigma_{T_m}}{T_m^2}\right)^2}. \quad (9)$$

[18] Then the total uncertainty of the GPS-derived IWV can be calculated by substituting equations (8) and (9) to equation (7).

[19] Table 1 gives examples of the calculated total uncertainties of the IWV for two GPS sites: BODS (–14.4°E, 67.3°N) and MEDI (11.7°E, 44.5°N). The heights above the mean sea level for the two sites are 9 and 19 m, respectively. The corresponding values for the IWV, the ZTD, the ground pressure P_0, and the mean temperature T_m were set to the mean values from the year of 2002 for each site. For comparison, we also used a larger value of 6 mm for the ZTD uncertainty. As shown in Table 1, the uncertainty in the estimated ZTD has the largest impact on the total IWV uncertainty. The uncertainty of the ZHD, caused by uncertainties of the ground pressure and the constant (2.2767 ± 0.0015 mm/hPa), has less impact but it is still significant.

[20] Later we present results for the monthly mean IWV, which has a smaller uncertainty due to the averaging of random errors. If the errors in individual IWV estimates are not at all correlated and there are no systematic errors, it is the uncertainty given for each IWV estimate divided by the square root of the number of IWV estimates for each month. However, this is not true for the GPS-derived IWV because it is subject to both random and systematic errors. Temporal correlations are seen in the errors in the GPS-derived ZTD [*Stoew et al*., 2007]. Using a 1 year long time series of the ZWD difference between the water vapor radiometer and GPS data at Onsala Space Observatory, *Stoew et al*. [2007] found that the decorrelation time of the ZWD difference is about 1 day. The possible systematic errors in the GPS-derived ZTD can be caused by many factors, e.g., satellite orbits errors and multipath effects. It is however difficult to distinguish the ZTD uncertainty due to systematic errors from the one caused by random errors. For each ZTD estimate, GIPSY provides a formal error which is largely dependent on the amount and distribution of carrier phase measurements for a given site, and does not account for systematic errors [*Jin et al*., 2006; *Byun and Bar-Sever*, 2009]. The mean formal error of the ZTD given by the GIPSY processing is around 3 mm for the investigated area.

[21] We adopt the 1 day decorrelation time and obtain 30 independent estimates for each month meaning that the formal uncertainty of the monthly mean is approximately $3/\sqrt{30}$ mm. All the other of the ZTD uncertainties are assumed to be caused by systematic errors, which are identical for the individual estimates and the monthly mean values.

[22] The ground pressure was taken from the ECMWF reanalysis product with assimilated observation data. Therefore, the errors in the observations, e.g., due to calibration

Table 1. Uncertainties of the GPS-Derived IWV Calculated From the Uncertainties Associated With Input Variables for Two GPS Sites: MEDI and BODS

Input Variable	MEDI	BODS	Uncertainty	Corresponding IWV Uncertainty					
				MEDI			BODS		
				[kg/m^2]	[%][h]	[%][i]	[kg/m^2]	[%][h]	[%][i]
ZTD [mm]	2438	2366	4[a]	0.63	3.1	70.2	0.61	5.8	71.8
			6	0.95	4.6		0.91	8.7	
Ground pressure P_0 [hPa]	1014.2	1009.1	0.9[b]	0.32	1.5	18.0	0.30	2.9	17.5
Constant[c] [mm/hPa]	2.2767	2.2767	0.0015	0.24	0.6	10.1	0.23	1.0	10.2
Mean temperature T_m [K]	278.3	267.9	1.1[d]	0.08	0.4	1.0	0.04	0.4	0.3
k'_2 [K/hPa]	22.1	22.1	2.2[e]	0.03	0.2	0.1	0.02	0.2	0.1
k_3 [$10^5 \times$ K^2/hPa]	3.739	3.739	0.012[e]	0.06	0.3	0.6	0.03	0.3	0.1
IWV [kg/m^2]	21	11							
Conversion factor Q	6.3	6.5							
Total IWV uncertainty (1)[f]				0.75	3.6		0.72	6.5	
Total IWV uncertainty (2)[g]				1.03	5.9		0.99	9.0	
Uncertainty of monthly mean (1)[f]				0.31	1.5		0.29	2.6	
Uncertainty of monthly mean (2)[g]				0.54	2.6		0.52	4.7	

[a]The claimed 1–σ uncertainty of the International GNSS Service ZTD product.
[b]Taken from *Heise et al*. [2009] based on the comparison between ECMWF reanalysis and ground measurement.
[c]The constant given in Equation (2).
[d]Taken from *Wang et al*. [2005] based on the comparison between ECMWF reanalysis and radiosonde data.
[e]Taken from Table 1 in *Bevis et al*. [1994].
[f]Calculated using 4 mm for the uncertainty of the ZTD.
[g]Calculated using 6 mm for the uncertainty of the ZTD.
[h]Calculated with respect to the IWV values of 21 kg/m^2 and 11 kg/m^2 for MEDI and BODS, respectively.
[i]Percentage of the total IWV uncertainty (1) is calculated by dividing the square of the uncertainty by the square of the total IWV uncertainty since the uncertainties are root-sum-square.

errors, are systematic for at least one day. Again we assumed that there are 30 estimates with independent errors when calculating the monthly mean uncertainty of the ground pressure. The uncertainty of the constant (2.2767 mm/hPa) is systematic for the whole data set. The calculated uncertainties of the monthly mean of the IWV for two sites are presented in Table 1. Given the insignificant impact of the uncertainties of T_m, k'_2, and k_3, they were neglected. Including them would only increase the monthly mean uncertainty by 3% for the worst case, i.e., if all three errors are systematic and if their absolute values are added.

4. Results

4.1. Assessment of Monthly Means

[23] The IWV obtained from RCA and from the reanalysis product of ECMWF were compared to the IWV from the GPS data. Model data were obtained from the nearest gridpoint to each GPS site. Given that the height difference between the grid box of the model and the GPS site can be the primary cause of the IWV difference [e.g., *Hagemann et al*., 2003; *Wang and Zhang*, 2009], it is necessary to refer the IWV value from models to the height of the GPS site. This was done by carrying out a cubic spline vertical interpolation using the lapse rate in the boundary layer. For each comparison, both the models and the GPS data were averaged over one month from their original temporal resolutions (GPS: 5 min; RCA: 30 min; ECMWF: 6 h). Due to gaps in the GPS data set, we only included those months with at least 15 days of data available to make the values representative for each month. The result was that 20% of the sites have no month excluded, while the number of excluded months are 1–2, 3–5, 6–10, and 10–13, for 59%, 13%, 6% and 2% of all the sites, respectively. Thereafter, we investigated the systematic effect introduced by gaps in the GPS data by comparing the model-derived IWV to the one obtained from the GPS data with and without including months with data gaps. We found differences less than 0.1 kg/m^2 in the mean IWV difference for all sites indicating that gaps in the GPS data introduce no significant systematic effect.

[24] Figures 2 and 3 depict examples of the time series of the monthly mean IWV and the difference between the GPS and the models' data for two sites, KIR0 (21.1°E, 67.9°N) and MATE (16.7°E, 40.7°N), with the heights above the mean sea level of 362 and 490 m, respectively. As expected, the results show a clear seasonal variation in the IWV time series, which is seen for both GPS and models. The mean IWV differences for the RCA-GPS comparisons are –0.28 kg/m^2 and –0.12 kg/m^2, respectively, while the corresponding standard deviations are 0.82 kg/m^2 and 1.30 kg/m^2. The mean IWV differences for ECMWF-GPS are 0.17 kg/m^2 and 0.52 kg/m^2 while the standard deviations are 0.26 kg/m^2 and 0.54 kg/m^2. As an example of detailed results comparisons for the year 2006 are shown in Figure 4. For the KIR0 site, a good correlation between the GPS and the ECMWF IWV is seen for the whole year, while a larger difference is seen from the RCA IWV for the month of August. For the site of MATE, larger IWV differences are seen in the summer for both RCA and ECMWF, but with the opposite sign. In order to investigate the seasonal variation of the monthly means

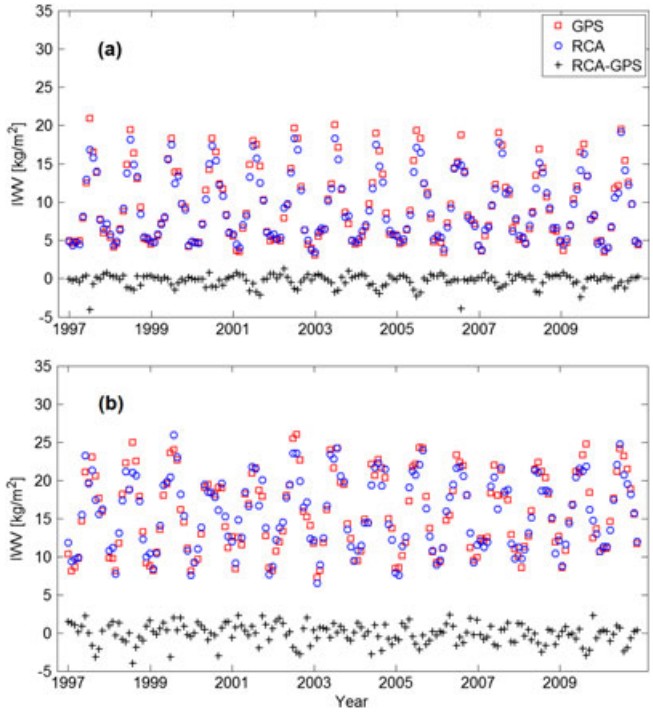

Figure 2. The time series of the monthly mean IWV and difference between RCA and GPS for the sites of (a) KIR0 and (b) MATE.

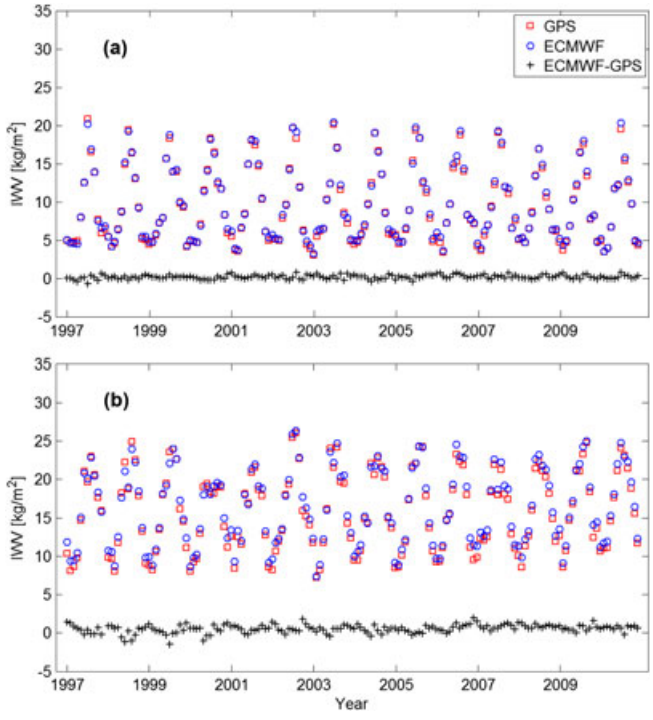

Figure 3. The time series of the monthly mean IWV and difference between ECMWF and GPS for the sites of (a) KIR0 and (b) MATE.

of the IWV difference, we calculated the mean IWV differences and standard deviations for each month, averaged over the whole 14 years and all the 99 sites. Figure 5

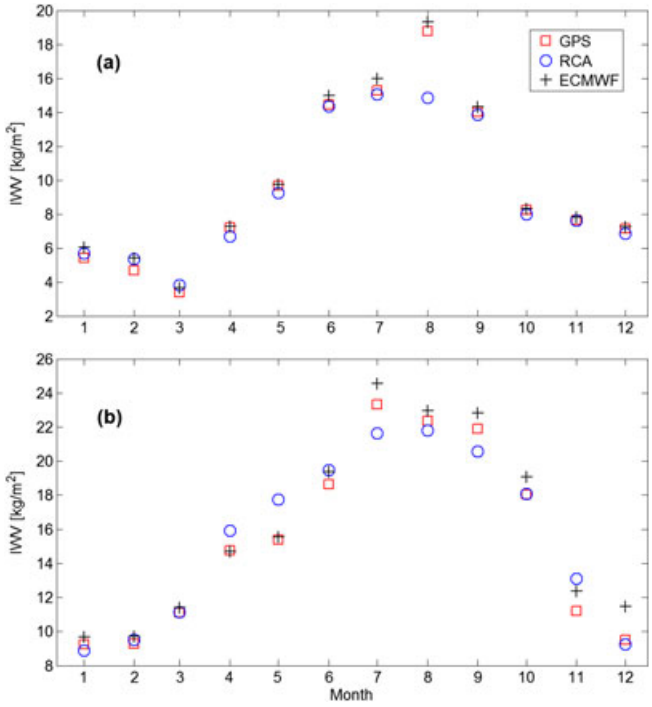

Figure 4. A close look on the monthly mean IWV for the year of 2006 and for the sites of (a) KIR0 and (b) MATE.

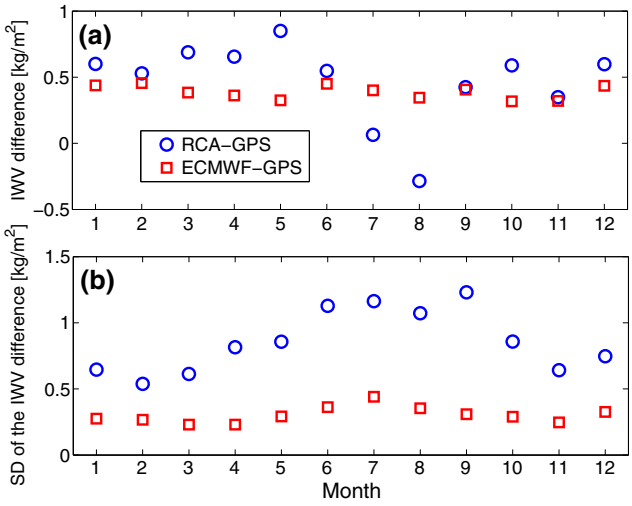

Figure 5. The mean IWV difference (a) and the standard deviation (SD) (b) shown for each month averaged over all 14 years and all the sites.

depicts a significant seasonal variation for RCA, which tends to underestimate IWV in the summer (July and August). In addition, the monthly standard deviation is larger in the summer for both RCA and ECMWF. We also carried out similar tests for different years and for different regions (see subsets in Table 2). All results demonstrate the same pattern as is seen in Figure 5.

[25] The mean IWV differences and standard deviations for individual sites are shown in Figures 6, 7, and 8. The mean IWV difference varies from –0.50 kg/m^2 to +1.09 kg/m^2 for RCA-GPS and from –0.21 kg/m^2 to +1.12 kg/m^2 for ECMWF-GPS. The differences seen for ECMWF are consistent with the results presented by *Heise et al.* [2009] for the European region. The two comparisons in Figure 6 result in similar patterns. However, a larger discrepancy is seen for two sites in Italy where ECMWF has a wet bias while RCA has a dry bias. This dry bias is in accordance with a cold temperature bias and an underestimate of the diurnal temperature range for the same region [*Samuelsson et al.*, 2011]. The lower temperature will lead to less surface evaporation and hence an underestimate of IWV. As expected, due to the fact that no observations were assimilated in RCA, the standard deviation of the IWV difference for RCA-GPS is approximately three times larger than the one for ECMWF-GPS (see Figures 7 and 8). A clear latitude dependence is seen in the standard deviation, which increases as the site latitude decreases due to larger IWV values (see Table 2).

[26] Table 2 presents statistics from the IWV comparisons for several subsets of the data. We investigated the impact of differences in vertical and horizontal position of the model gridpoint as well as the model surface type. Averaged over all 99 sites and the whole 14 years, monthly mean IWV differences of 0.47 kg/m^2 and 0.39 kg/m^2 (relative difference of 3.5% and 2.9%) were obtained for RCA-GPS and ECMWF-GPS, respectively. The corresponding standard deviations were 0.98 kg/m^2 and 0.35 kg/m^2 (relative standard deviations of 7.4% and 2.6%). No changes in the results were seen when we used a subset of the data from the last 7 years (2004–2010). Slightly larger standard deviations are seen for both models for the sites south of 55°N. Statistics for the sites with the height difference between GPS and models, larger or smaller than 100 m, do not show significant differences. The horizontal difference between the closest model gridpoint and the GPS site, larger and smaller than 17 km, shows no impact, neither on the bias nor on the standard deviation.

[27] Sites close to the sea, where the surface tile of the model gridpoint has more than 60% water coverage, have a larger mean IWV difference for RCA and a slightly larger value for ECMWF compared to sites further away from the sea. This is likely due to the fact that the model gridpoint surface flux, such as evaporation, is a mean value calculated from each sub tile for the different surface types as described in section 2.2. Because the evaporation is larger from a water surface, it will dominate the mean value and can affect the mean IWV for such points when comparing to a GPS site on land.

4.2. Assessment of Temporal and Spatial Variability in IWV

[28] The diurnal cycle is one of the most obvious and reliable signals reflecting the solar variation throughout the day. Given its high temporal resolution, GPS-derived IWV is valuable for evaluating the ability of climate models to capture the diurnal cycles. Figure 9 depicts the diurnal cycles of IWV for the summer months, June, July, and August, as a function of the local solar time (LST) averaged for all sites using data from GPS, RCA, and ECMWF. The RCA captures the diurnal cycle reasonably well but with a later phase and a smaller amplitude. The mean peak time is at 18 LST compared to the mean peak time of the GPS at

Table 2. Statistics From the Comparisons of the IWV Between Models and GPS

Subset	Mean GPS IWV [kg/m^2]	Mean Difference [kg/m^2]	Mean Difference [%][a]	Standard Deviation [kg/m^2]	Standard Deviation [%][a]
All sites for the whole 14 years (1997–2010)					
RCA-GPS	13.33	0.47	3.5	0.98	7.4
ECMWF-GPS	13.33	0.39	2.9	0.35	2.6
All sites for the last 7 years (2004–2010))					
RCA-GPS	13.37	0.47	3.5	0.98	7.3
ECMWF-GPS	13.37	0.42	3.1	0.34	2.5
75 sites with the latitude north of 55°N					
RCA-GPS	12.64	0.48	3.8	0.95	7.5
ECMWF-GPS	12.64	0.40	3.2	0.33	2.6
24 sites with the latitude south of 55°N					
RCA-GPS	15.51	0.42	2.7	1.09	7.0
ECMWF-GPS	15.51	0.36	2.3	0.42	2.7
56 sites with the horizontal distance larger than 17 km[b]					
RCA-GPS	13.53	0.48	3.6	0.97	7.2
ECMWF-GPS	13.53	0.35	2.6	0.35	2.6
43 sites with the horizontal distance smaller than 17 km[b]					
RCA-GPS	13.08	0.45	3.4	0.99	7.6
ECMWF-GPS	13.08	0.43	3.3	0.35	2.7
17 sites with the height difference larger than 100 m					
RCA-GPS	12.23	0.41	3.4	0.89	7.3
ECMWF-GPS	12.23	0.46	3.8	0.41	3.4
82 sites with the height difference smaller than 100 m					
RCA-GPS	13.56	0.48	3.5	1.00	7.4
ECMWF-GPS	13.56	0.37	2.7	0.34	2.5
23 sites with the water coverage larger than 60%[c]					
RCA-GPS	13.42	0.62	4.6	0.93	6.9
ECMWF-GPS	13.42	0.46	3.4	0.33	2.5
76 sites with the water coverage smaller than 60%[c]					
RCA-GPS	13.31	0.42	3.2	1.00	7.5
ECMWF-GPS	13.31	0.36	2.7	0.36	2.7

[a]Percentage of the mean GPS IWV.
[b]The horizontal distance between the GPS site and the closest model gridpoint.
[c]The GPS sites where the surface tile of the model gridpoint has a water coverage larger, or smaller, than 60% (see text).

17 LST. The smaller amplitude is mainly due to larger nighttime values. The amplitude and phase differences may partly be explained by that the model value is an average over 50 × 50 km and a time step of 30 min whereas the GPS data represent one point with a time step of 5 min. The differences in amplitude and phase may, however, also be due to errors in the convective and surface parameterizations, as found by *Jeong et al*. [2011] investigating the RCA diurnal cycle of precipitation. For ECMWF, we only have values every 6 h, but as for RCA, the IWV amplitude is smaller and the mean value is higher both for the night and the day compared to the GPS data. The variation of the peak

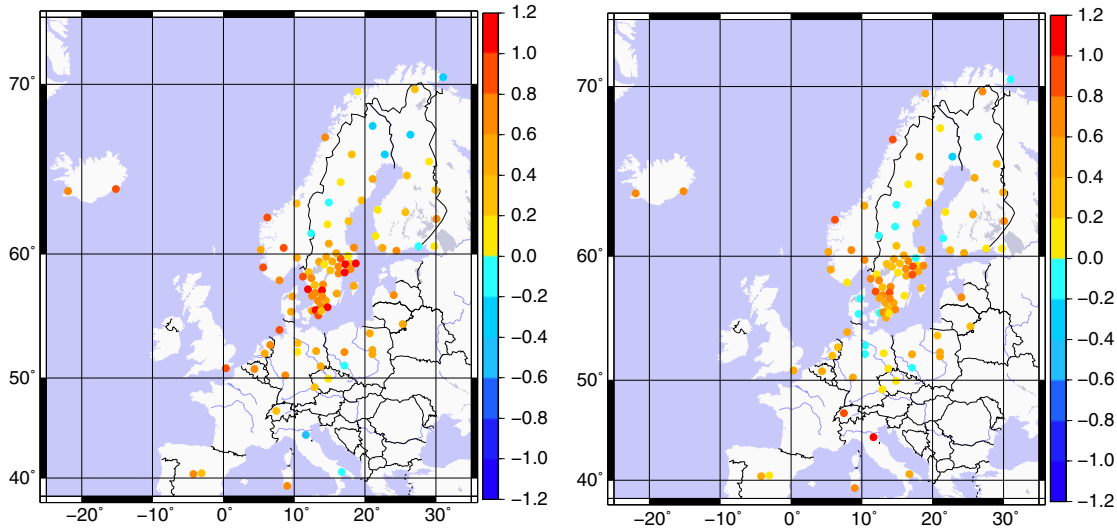

Figure 6. The mean IWV difference (kg/m^2) for (left) RCA-GPS and (right) ECMWF-GPS.

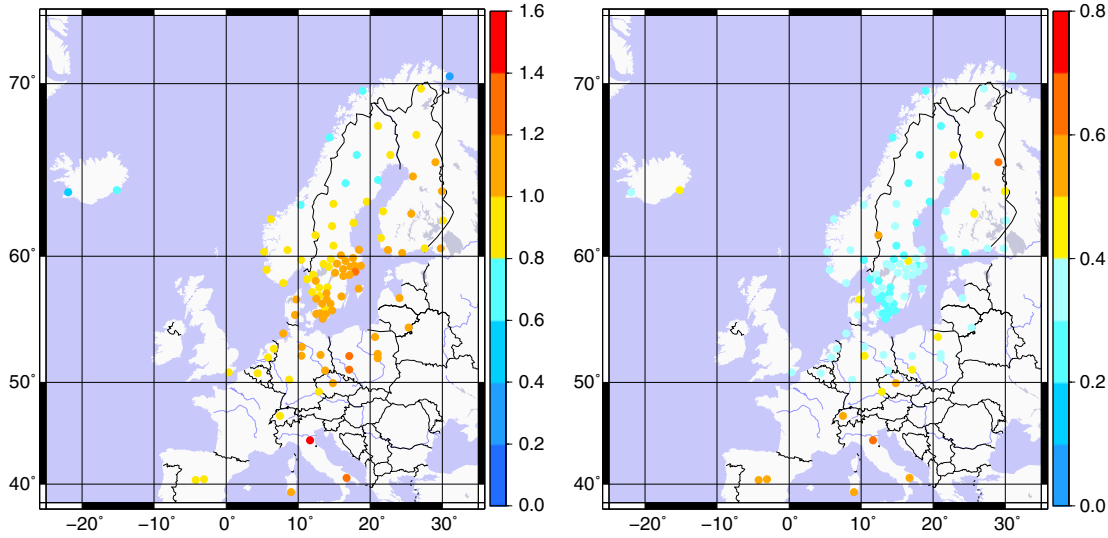

Figure 7. The standard deviation of the IWV difference (kg/m^2) for (left) RCA-GPS and (right) ECMWF-GPS. Note that a different scale is used for the ECMWF-GPS comparison.

time of the diurnal cycle for each site for the summer months is shown in Figure 10 where a clear positive correlation is seen between GPS and RCA. The peak varies from 16 to 19 LST for the GPS data while there is a dominant peak at 18 LST for the RCA data. The RCA captures the geographical variations from west to east, with later peaks in the afternoon further east, and the late night and early morning peaks along the east coast of Sweden. These coastal IWV outliers may be related to the observed and modeled peaks in precipitation in early morning at 4–7 A. M. found by *Jeong et al*. [2011], which they suggested could be linked to deep convection development over the Baltic Sea. Future studies with a high horizontal resolution model of 2–3 km will enable a study of these local effects and also help to investigate the differences in the GPS and modeled IWV.

[29] The GPS data can also be used to investigate the spatial variability of the IWV. As discussed in section 3, satellite orbit errors are one of factors which significantly contribute to the uncertainty of the GPS-derived IWV. However, GPS sites in a small network have almost the same geometry of the satellite constellation and therefore an orbit error introduces a similar offset in the IWV. As a result, a reduced impact of such errors occurs when we calculate the spatial structure function of the IWV, which is defined as

$$D_V = < \left[V\left(\vec{X} + \vec{\rho}\right) - V\left(\vec{X}\right) \right]^2 > \qquad (10)$$

where V is the IWV at the sites, $\vec{X}$ is the position of the first site; $\vec{\rho}$ is the vector between the two sites; and the angle brackets denote the expectation value.

[30] We have a dense subnetwork in the region between latitudes 55°N and 61°N, and between longitudes 11°E and 19°E (see Figure 1). We used these GPS data to

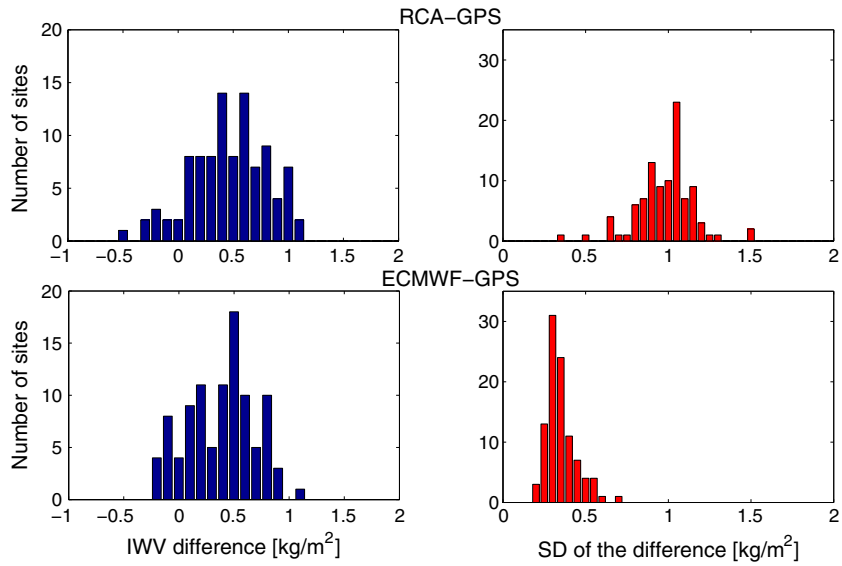

Figure 8. Histograms of the mean IWV difference and the standard deviation (SD) for all sites.

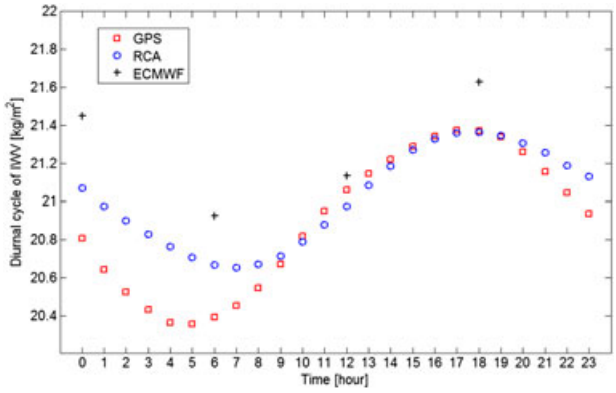

Figure 9. Diurnal cycles of IWV as a function of local solar time for the summer months (JJA) obtained from the data for all sites and all years.

calculate the spatial structure function of the IWV and compared it to the one obtained from the models for the same sites. In order to investigate the impact due to different horizontal resolution in the model, the spatial structure function of the IWV was also calculated using an RCA simulation run with a higher horizontal resolution of 11 km. Figures 11 and 12 depict D_V as a function of the distance $|\vec{\rho}|$. There is a better agreement between the GPS and the RCA structure functions, indicating that the RCA data reflect the atmospheric spatial variations better than the ECMWF reanalysis. This is expected since the resolution used in the ECMWF was only 2°. In addition, a smaller and also relatively distance independent difference is seen for the 11 km horizontal resolution (see Figure 12b). The least squares estimates of the power-law dependence of D_V on $\vec{\rho}$ are 1.0, 1.2, and 1.3 for the GPS, the RCA, and the ECMWF data, respectively when we used the models' data with a 50 km horizontal resolution. The corresponding result using RCA with an 11 km resolution is 1.0. The result indicates that a higher horizontal resolution can improve the ability of a regional climate model to reflect the spatial variation of the IWV.

5. Conclusions

[31] The atmospheric IWV in a regional climate model (RCA) is evaluated using ground-based GPS measurements from 99 European sites, each with a maximum time series of 14 years. We also used the reanalysis product of ECMWF. Averaged over all the sites and the 14 years IWV differences of 0.47 kg/m^2 and 0.39 kg/m^2 relative to the GPS monthly means are obtained for RCA and ECMWF, respectively. The IWV difference for individual sites varies from –0.50 kg/m^2 to +1.09 kg/m^2 for RCA-GPS and from –0.21 kg/m^2 to +1.12 kg/m^2 for ECMWF-GPS. The corresponding standard deviations are 0.98 kg/m^2 and 0.35 kg/m^2. The standard deviation for RCA-GPS is approximately three times larger than the standard deviation for ECMWF-GPS due to the fact that no observations were assimilated in RCA.

[32] The IWV difference for RCA is positively correlated to the difference for ECMWF. However, this is not the case

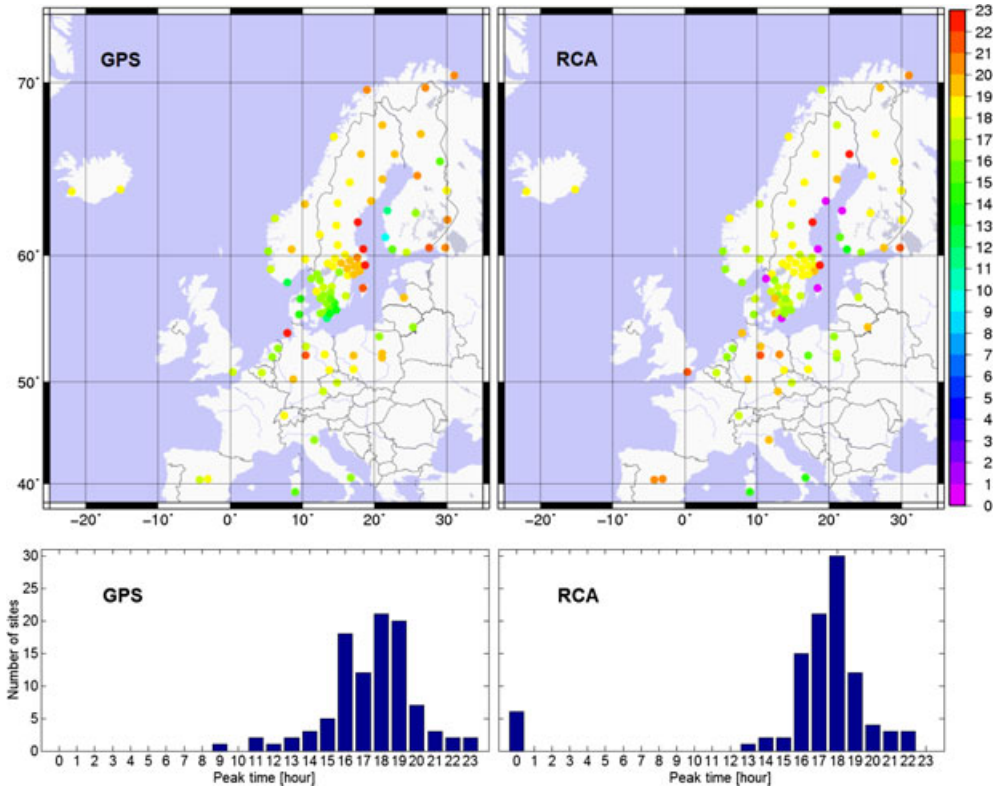

Figure 10. Peak time of the diurnal cycle of the IWV, for the summer months (JJA), obtained from the GPS data and the RCA simulation for each GPS site (upper panels) and histograms of the peak time (lower panels). The hour is in local solar time.

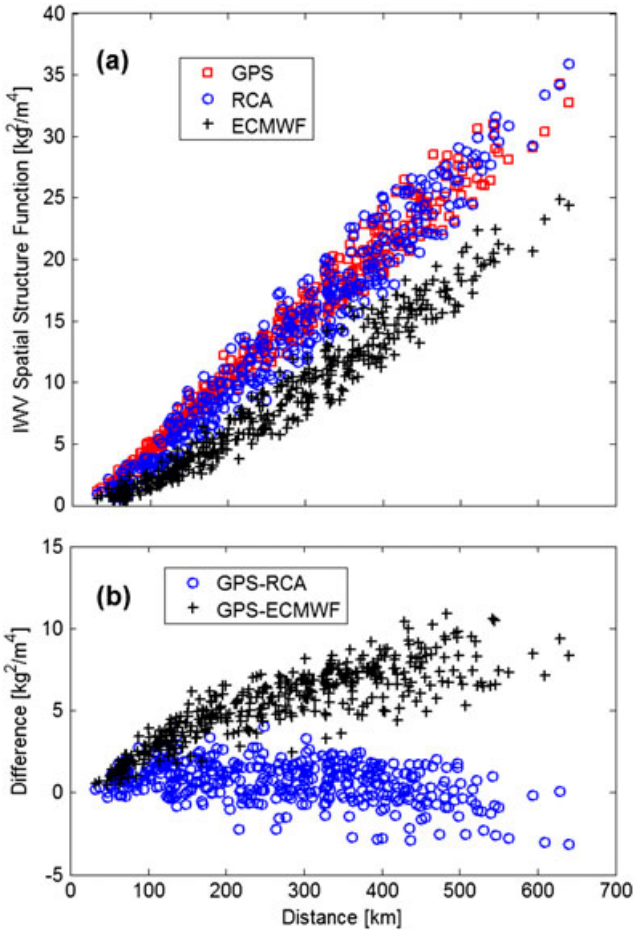

Figure 11. (a) Spatial structure functions of the IWV for the dense GPS network from both models and GPS data, and (b) the difference. The horizontal resolution in the models is 50 km.

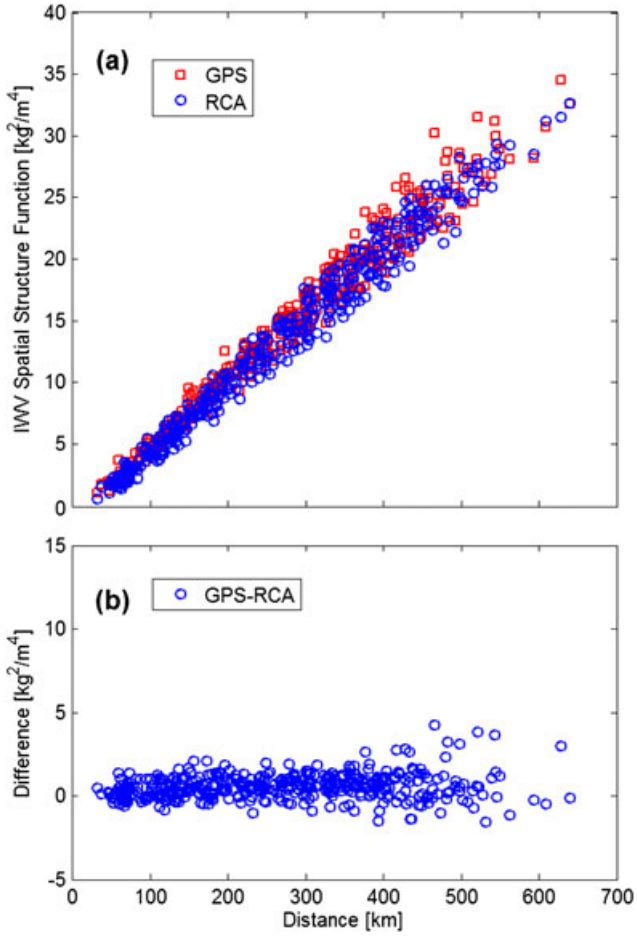

Figure 12. (a) Spatial structure functions of the IWV for the dense GPS network from the RCA and the GPS data, and (b) the difference. The horizontal resolution in RCA is 11 km.

for two sites in Italy where a wet bias is seen for ECMWF and a dry bias is seen for RCA. The dry bias seen in the RCA is in accordance with a cold temperature bias found for the same region [*Samuelsson et al*., 2011].

[33] Models tend to give a larger IWV (more significant for the RCA model) for the sites nearby sea where the surface tile of the model gridpoint has a water coverage larger than 60%. This may be due to that the IWV value obtained from models is the mean for the gridbox. The result indicates that care has to be taken when comparing the GPS data to the model gridded output.

[34] Comparing the diurnal cycles of the IWV show that the RCA captures the diurnal cycle but has a smaller amplitude, due to a higher nighttime value, and a slightly later peak time (18 LST instead of 17 LST for GPS). The geographical variation of the peak time was fairly well captured by the model.

[35] Using a subset of the data, from a dense GPS network, we compare the GPS and the RCA IWV in terms of representing the spatial variability. A horizontal resolution of 11 km, instead of 50 km, in the RCA results in a significantly better agreement.

[36] **Acknowledgments.** We would like to thank Erik Kjellström for his valuable comments. This research was supported by VINNOVA, the Swedish Governmental Agency for Innovation Systems, through the project P29459-1 "Long Term Water Vapour Measurements Using GPS for Improvement of Climate Modelling". The maps in Figures 1, 6, 7, and 10 were produced using the Generic Mapping Tools [*Wessel and Smith*, 1998].

References

Askne, J., and H. Nordius (1987), Estimation of tropospheric delay for microwaves from surface weather data, *Radio Sci.*, *22*, 379–386, doi:10.1029/RS022i003p00379.

Bengtsson, L., S. Hagemann, and K. I. Hodges (2004), Can climate trends be calculated from reanalysis data?, *J. Geophys. Res.*, *109*, D11111, doi:10.1029/2004JD004536.

Bevis, M., S. Chiswell, T. A. Herring, R. A. Anthes, C. Rocken, and R. H. Ware (1994), GPS meteorology: Mapping zenith wet delays onto precipitable water, *J. Appl. Meteorol.*, *33*, 379–386, doi:10.1175/1520-0450(1994)033 < 0379:GMMZWD > 2.0.CO;2.

Byun, S., and Y. Bar-Sever (2009), A new type of troposphere zenith path delay product of the international GNSS service, *J. Geod.*, *83* (3), 367–373, doi:10.1007/s00190-008-0288-8.

Cess, R. D., et al. (1990), Intercomparison and interpretation of climate feedback processes in atmospheric general circulation models, *J. Geophys. Res.*, *95*, 16,601–16,615, doi:10.1029/90JD01219.

Chaboureau, J. -P., A. Chédin, and N. A. Scott (1998), Remote sensing of the vertical distribution of atmospheric water vapor from the TOVS observations: Method and validation, *J. Geophys. Res.*, *103*(D8), 8,743–8,752, doi:10.1029/98JD00045.

Davies, H. C. (1976), A lateral boundary formulation for multi-level prediction models, *Q. J. R. Meteorol. Soc.*, *102*, 405–418, doi:10.1002/qj.49710243210.

Davis, J. L., T. A. Herring, I. I. Shapiro, A. E. E. Rogers, and G. Elgered (1985), Geodesy by radio interferometry: Effects of atmospheric

modeling errors on estimates of baseline length, *Radio Sci.*, *20*, 1593–1607, doi:10.1029/RS020i006p01593.

Dee, D. P., et al. (2011), The ERA-Interim reanalysis: configuration and performance of the data assimilation system. *Q. J. R. Meteorol. Soc.*, *137*:553–597. doi:10.1002/qj.828.

Elgered, G. (1993), Tropospheric radio path delay from ground-based microwave radiometry, *in Atmospheric Remote Sensing By Microwave Radiometry*, Wiley & Sons Inc, pp. 215–258, New York, N. Y.

Gradinarsky, L. P., J. Johansson, H. R. Bouma, H-G. Scherneck, and G. Elgered (2002), Climate monitoring using GPS, *Phys. Chem. Earth.*, *27*, 225–340, doi:10.1016/S1474-7065(02)00009-8.

Hagemann, S., L. Bengtsson, and G. Gendt (2003), On the determination of atmospheric water vapor from GPS measurements, *J. Geophys. Res.*, *108* (D21), 4,678, doi:10.1029/2002JD003235.

Held, I. M., and B. J. Soden (2000), Water vapor feedback and global warming, *Ann. Rev. of Energy and the Environment*, *25*, 441–475, doi:10.1146/annurev.energy.25.1.441.

Heise, S., G. Dick, G. Gendt, T. Schmidt, and J. Wickert (2009), Integrated water vapor from IGS ground-based GPS observations: initial results from a 5-min data set, *Ann. Geophys.*, *27*, 2,851–2,859, doi:10.5194/angeo-27-2851-2009.

Jeong, J. -H., A. Walther, G. Nikulin, D. Chen, and C. Jones (2011), Diurnal cycle of precipitation amount and frequency in Sweden: observation versus model simulation, *Tellus A*, *63*:664–674, doi:10.1111/j.1600-0870.2011.00517.x.

Jin, S., J.-U. Park, P.-H. Park, and J. -H. Cho (2006), Modelling Systematic Residuals in Absolute ZTD Estimation from GPS, *Geoscience and Remote Sensing Symposium, IGARSS 2006*, 2,623–2,626, doi:10.1109/IGARSS.2006.677.

Jones, C. G., U. Willén, A. Ullerstig, and U. Hansson (2004), The Rossby Centre Regional Atmospheric Climate Model Part I: Model climatology and performance for the present climate over Europe, *Ambio*, *33*, 199–210.

Jury, M. R., and D. Waliser (1990), Satellite microwave measurements of atmospheric water vapour and marine wind speed: case study application, *S. Afr. J. mar. Sci.*, *9*, 309–316, doi:10.2989/025776190784378943.

Lyard F., F. Lefevre, T. Letellier, and O. Francis (2006), Modelling the global ocean tides: Modern insights from FES2004, *Ocean Dyn.*, *56*(5), 394–415, doi:10.1007/s10236-006-0086-x.

Niell, A. E. (1996), Global mapping functions for the atmosphere delay at radio wavelengths, *J. Geophys. Res.*, *101*, 3,227–3,246, doi:10.1029/95JB03048.

Ning, T., R. Haas, and G. Elgered (2012), Multi-Technique Comparisons of Ten Years of Wet Delay Estimates on the West Coast of Sweden, *J. Geod.*, *86*(7), 565–575, doi:10.1007/s00190-011-0527-2.

Ross, R. J., and W. P. Elliott (1996), Tropospheric water vapor climatology and trends over north America: 1973–93, *J. Climate*, *9*, doi:10.1175/1520-0442(1996)009 < 3561:TWVCAT > 2.0.CO;2, 3,561–3,574.

Ross, R. J., and W. P. Elliott (2001), Radiosonde-based Northern Hemisphere tropospheric water vapor trends, *J. Clim.*, *14*, 1,602–1,612, doi:10.1175/1520-0442(2001)014 < 1602:RBNHTW > 2.0.CO;2.

Saastamoinen, J. (1973), Contributions to the theory of atmospheric refraction, *Bull. Géod.*, *107*, 13–34, doi:10.1007/BF02521844.

Samuelsson, P., S. Gollvik, and A. Ullerstig A (2006), The land-surface scheme of the Rossby Centre regional atmospheric climate model (RCA3), *Report in Meteorology 122*, SMHI. SE-601 76 Norrköping, Sweden.

Samuelsson, P., C. Jones, U. Willén, A. Ullerstig, S. Gollvik, U. Hansson, E. Kjellström, G. Nikulin, and K. Wyser (2011), The Rossby centre regional climate model RCA3: model description and performance, *Tellus A.*, *63*, 4–23, doi:10.1111/j.1600-0870.2010.00478.x.

Semenov, V. A., and L. Bengtsson (2002), Secular trends in daily precipitation characteristics: Greenhouse gas simulation with a coupled AOGCM, *Clim. Dyn.*, *19*, 123–140, doi:10.1007/s00382-001-0218-4.

Schmid, R., P. Steigenberger, G. Gendt, M. Ge, and M. Rothacher (2007), Generation of a consistent absolute phase center correction model for GPS receiver and satellite antennas, *J. Geod.*, *81*, 781–798, doi:10.1007/s00190-007-0148-y.

Stoew, B., T. Nilsson, G. Elgered, and P. O. J. Jarlemark (2007), Temporal correlations of atmospheric mapping function errors in GPS estimation, *J. Geod.*, *81*(5), 311–323, doi:10.1007/s00190-006-0114-0.

Titchner, H. A., P. W. Thorne, M. P. McCarthy, S. F. B. Tett, L. Haimberger, and D. E. Parker (2009), Critically reassessing tropospheric temperature trends from radiosondes using realistic validation experiments, *J. Clim.*, *22*, 465–485, doi:10.1175/2008JCLI2419.1.

Thomas, I. D., M. A. King, P. J. Clarke, and N. T. Penna (2011), Precipitable water vapor estimates from homogeneously reprocessed GPS data: An intertechnique comparison in Antarctica, *J. Geophys. Res.*, *116*, doi:10.1029/2010JD013889.

Trenberth, K. E., et al. (2005), Trends and variability in column-integrated atmospheric water vapor, *Clim. Dyn.*, *24*, 741–758, doi:10.1007/s00382-005-0017-4.

Undén, P., et al. (2002), HIRLAM-5 scientific documentation, *HIRLAM Report*, SMHI, SE-601 76 Norrköping, Sweden.

Uppala, S. M., et al. (2005), The ERA-40 re-analysis, *Quart. J. R. Meteorol. Soc.*, *131*, 2,961–3,021, doi:10.1256/qj.04.176.

Vey, S., R. Dietrich, M. Fritsche, A. Rülke, P. Steigenberger, and M. Rothacher (2009), On the homogeneity and interpretation of precipitable water time series derived from global GPS observations, *J. Geophys. Res.*, *114*, D10101, doi:10.1029/2008JD010415.

Vey, S., R. Dietrich, A. Rülke, M. Fritsche, P. Steigenberger, M. Rothacher (2010), Validation of Precipitable Water Vapor within the NCEP/DOE Reanalysis Using Global GPS Observations from One Decade, *J. Climate*, *23*, 1,675–1,695. doi:10.1175/2009JCLI2787.1.

Wang, J., L. Zhang, and A. Dai (2005), Global estimates of water-vapor-weighted mean temperature of the atmosphere for GPS applications, *J. Geophys. Res.*, *110*, D21101, doi:10.1029/2005JD006215.

Wang, J., and L. Zhang (2008), Systematic errors in global radiosonde precipitable water data from comparisons with ground-based GPS measurements, *J. Clim.*, *21*(10), 2,218–2,238, doi:10.1175/2007JCLI1944.1.

Wang, J., and L. Zhang (2009), Climate applications of a global, 2-hourly atmospheric precipitable water dataset from IGS round-based GPS measurements, *J. Geod.*, *83*, 209–217, doi:10.1007/s00190-008-0238-5.

Webb, F. H., and J. F. Zumberge (1993), *An Introduction to the GIPSY/OASIS-II*, JPL Publ. D-11088, Jet Propulsion Laboratory, Pasadena, California.

Wessel, P. and W. H. F. Smith (1998), New, improved version of generic mapping tools released, *EOS Trans. Amer. Geophys. U.*, *79*(47), 579, doi:10.1029/98EO00426.

Wyser, K., et al. (2008), An evaluation of Arctic cloud and radiation processes during the SHEBA year: simulation results from eight Arctic regional climate models, *Clim. Dyn.*, *30*, 203–223, doi:10.1007/s00382-007-0286-1.

Zumberge, J. F., M. B. Heflin, D. C. Jefferson, M. M. Watkins, and F. H. Webb (1997), Precise Point Positioning for the Efficiet and Robust Analysis of GPS Data from Large Networks, *J. Geophys. Res.*, *102* (B3), 5,005–5,017, doi:10.1029/96JB03860.